NOTE: Use these buttons to print or save the form. DO NOT use the browser tool bar. SAVE PRINT

LA-UR- 05-1542

Approved for public release; distribution is unlimited.

Title:	Numerical Moments Computation for CAPS/IMS
Author(s):	Michelle F. Thomsen, ISR-1 Dorothea M. Delapp, ISR-1
Submitted to:	An unpublished report available for unlimited distribution from the CAPS web page

SAVE PRINT CLEAR FORM

Los Alamos NATIONAL LABORATORY

Numerical Moments Computation for CAPS/IMS

M. F. Thomsen and D. M. Delapp

24 February 2005

Abstract

This report described the theoretical and computational approach developed at Los Alamos to calculate moments of the ion distribution observed at Saturn by the CAPS/IMS, as reported in the SNG data product. The approximations, assumptions, procedures, and instrument parameters that go into the calculation are presented, as well as caveats about the applicability of the results. The calculations described here are carried out in the code MOM_SNG_NUM, Rev. 0, dated 18 Mar 2005.

Table of Contents

I. *Theoretical Approach*

The moments we would like to compute from CAPS measurements are the density, vector flow velocity, and temperature tensor, defined respectively as

$$n = \int_{all\ \mathbf{v}} f(\mathbf{v})\, d^3\mathbf{v} \tag{1a}$$

$$\mathbf{V} = \left(1/n\right) \int_{all\ \mathbf{v}} \mathbf{v}\, f(\mathbf{v})\, d^3\mathbf{v} \tag{1b}$$

$$\underline{\underline{\mathbf{T}}} = \left(m/n\right) \int_{all\ \mathbf{v}} (\mathbf{v}-\mathbf{V})(\mathbf{v}-\mathbf{V})\ f(\mathbf{v})\, d^3\mathbf{v} \tag{1c}$$

The computation of moments by numerical integration over the observed distribution normally requires that the full 4π of velocity space be measured. Because of the limited field of view of the CAPS instrument, even when the actuator is in full operation, simple numerical integration of the observed distribution would lead to biased results. The density would obviously be underestimated, particularly if the flow is subsonic, but with an accurate knowledge of the flow velocity, much of the missing distribution could be reconstructed by symmetry arguments such as are used in the GSFC algorithm. The

biggest problem under these circumstances is the estimation of the velocity: With only one side of the distribution observed, a simple velocity-weighted numerical integration of the observed counts will artificially force the derived velocity to lie within the instrument FOV and will overestimate its magnitude even if the true velocity does lie within the observed part of velocity space.

One solution to this problem is to use a functional fit to the distribution, rather than a numerical integration. Our preliminary moments code (Thomsen/Delapp) fits the observed counts to an isotropic, convecting Maxwellian. In principle, this approach has the advantage that it does not require the full distribution (or even a velocity-balanced portion of it) to be measured. In practice, it has the disadvantages of being model-dependent, of being rather unstable (it sometimes finds a solution with the velocity well out of the observed range of velocity space), and most troublesome, of coupling the temperature and velocity. The latter problem appears for example when the "cross-talk" caused by scattering into adjacent detectors is not adequately removed; the result is an overestimate of the temperature, which forces an underestimate of the flow velocity (since the average energy of the observed distribution is robustly determined).

The approach used in the GSFC code is to find the point in velocity space from which the observed distribution gives zero net flux. Because of the imbalance in velocity space coverage by CAPS, the GSFC method mirrors any unbalanced observation points about the trial bulk velocity, thereby enforcing balance and a zero contribution to the net flux from such unbalanced points. An equivalent alternative is simply to exclude such unbalanced points entirely from the net flux calculation, and this is the basis on which we build our code. The approach described below ought to give very similar results to the Goddard approach.

The moments we are interested in are all integrals of the form

$$M = \int_{all\ \mathbf{v}} g(\mathbf{v})\, f(\mathbf{v})\, d^3\mathbf{v} \qquad (2)$$

where $f(\mathbf{v})$ is the velocity distribution function, and the velocity functions $g(\mathbf{v})$ are related to the desired moments:

$g(\mathbf{v}) = 1$	->	density
$g(\mathbf{v}) = \mathbf{v}$	->	velocity
$g(\mathbf{v}) = \mathbf{vv}$	->	temperature

The integral in Equation 2 is to be taken over the entire volume of velocity space, which is comprised of the part that CAPS views (*obs*) and the part CAPS does not view (*unobs*):

$$M = \int_{all\ \mathbf{v}} g(\mathbf{v})\, f(\mathbf{v})\, d^3\mathbf{v} = \int_{obs} g(\mathbf{v})\, f(\mathbf{v})\, d^3\mathbf{v} + \int_{unobs} g(\mathbf{v})\, f(\mathbf{v})\, d^3\mathbf{v} \qquad (3)$$

To proceed, we will invoke the presumed symmetry of the velocity distribution function in the reference frame moving with the flowing plasma. Specifically, we will assume that the distribution is mirror symmetric about the flow velocity **V**. Thus, we assume that

$$f(2\mathbf{V}-\mathbf{v}) = f(\mathbf{v}) \tag{4}$$

If we knew the actual velocity **V** of the plasma, we could divide the observed volume of velocity space into a "symmetric" portion (*sym*), containing those observation points whose mirrored (about **V**) points are also contained in the observed volume of velocity space, and an "unbalanced" portion (*unbal*), containing observed measurement points whose mirrored values do not lie within the observed space. Then, Equation 3 becomes

$$M = \int_{sym} g(\mathbf{v}) f(\mathbf{v}) d^3\mathbf{v} + \int_{unbal} g(\mathbf{v}) f(\mathbf{v}) d^3\mathbf{v} + \int_{unobs} g(\mathbf{v}) f(\mathbf{v}) d^3\mathbf{v}$$

The unobserved portion of velocity space also consists of two parts: 1) the mirror of the unbalanced portion, and 2) a remainder:

$$M = \int_{sym} g(\mathbf{v}) f(\mathbf{v}) d^3\mathbf{v} + \int_{unbal} g(\mathbf{v}) f(\mathbf{v}) d^3\mathbf{v} + \int_{mir\ unbal} g(\mathbf{v}) f(\mathbf{v}) d^3\mathbf{v} + Rem \tag{5}$$

We now assume that compared to the amount of the distribution contained in the *sym, unbal,* and *mir unbal* portions of velocity space, the remainder term is negligible, giving our adopted moment equation:

$$M \cong \int_{sym} g(\mathbf{v}) f(\mathbf{v}) d^3\mathbf{v} + \int_{unbal} g(\mathbf{v}) f(\mathbf{v}) d^3\mathbf{v} + \int_{mir\ unbal} g(\mathbf{v}) f(\mathbf{v}) d^3\mathbf{v} \tag{6}$$

With the assumption of mirror symmetry, Equation 4, the integral over *mir unbal* can be related to the integral over *unbal*:

$$\int_{mir\ unbal} g(\mathbf{v}') f(\mathbf{v}') d^3\mathbf{v}' = \int_{unbal} g(2\mathbf{V} - \mathbf{v}) f(\mathbf{v}) d^3\mathbf{v} \tag{7}$$

For the moments of interest, we therefore have the following expressions for the three contributions in Equation 6:

for $g(\mathbf{v}) = 1$,

$$\eta_s \equiv \int_{sym} f(\mathbf{v}) d^3\mathbf{v} \tag{8a}$$

$$\eta_u \equiv \int_{unbal} f(\mathbf{v}) d^3\mathbf{v} \tag{8b}$$

$$\eta_m \equiv \int_{mir\ unbal} f(\mathbf{v}) d^3\mathbf{v} = \int_{unbal} f(\mathbf{v}) d^3\mathbf{v} = \eta_u \tag{8c}$$

for $g(\mathbf{v}) = \mathbf{v}$,

$$\mathbf{j}_s \equiv \int_{sym} \mathbf{v} f(\mathbf{v}) d^3\mathbf{v} \tag{9a}$$

$$\mathbf{j}_u \equiv \int_{unbal} \mathbf{v} f(\mathbf{v}) d^3\mathbf{v} \tag{9b}$$

$$\mathbf{j}_m \equiv \int_{mir\ unbal} \mathbf{v} f(\mathbf{v}) d^3\mathbf{v} = \int_{unbal} (2\mathbf{V} - \mathbf{v}) f(\mathbf{v}) d^3\mathbf{v} = 2\eta_u \mathbf{V} - \mathbf{j}_u \tag{9c}$$

and for $g(\mathbf{v}) = \mathbf{vv}$,

$$\underline{\underline{\tau}}_s \equiv \int_{sym} \mathbf{vv} f(\mathbf{v}) d^3\mathbf{v} \tag{10a}$$

$$\underline{\underline{\tau}}_u \equiv \int_{unbal} \mathbf{vv} f(\mathbf{v}) d^3\mathbf{v} \tag{10b}$$

$$\underline{\underline{\tau}}_m \equiv \int_{mir\ unbal} \mathbf{vv} f(\mathbf{v}) d^3\mathbf{v} = \int_{unbal} (2\mathbf{V} - \mathbf{v})(2\mathbf{V} - \mathbf{v}) f(\mathbf{v}) d^3\mathbf{v}$$
$$= 4\eta_u \mathbf{VV} - 2\mathbf{V}\mathbf{j}_u - 2\mathbf{j}_u\mathbf{V} + \underline{\underline{\tau}}_u \tag{10c}$$

Remembering that the sum of the *sym* and *unbal* volumes of velocity space are equal to the total observed volume (*obs*), we can further define the corresponding integrals over *obs*:

$$\eta_o \equiv \int_{obs} f(\mathbf{v}) d^3\mathbf{v} = \eta_s + \eta_u \tag{11a}$$

$$\mathbf{j}_o \equiv \int_{obs} \mathbf{v} f(\mathbf{v}) d^3\mathbf{v} = \mathbf{j}_s + \mathbf{j}_u \tag{11b}$$

$$\underline{\underline{\tau}}_o \equiv \int_{obs} \mathbf{vv} f(\mathbf{v}) d^3\mathbf{v} = \underline{\underline{\tau}}_s + \underline{\underline{\tau}}_u \tag{11c}$$

We then use Equations 11a-c and Equations 8-10 to express the desired moments (Equation 1) in terms of *obs* and *sym* quantities.

The density is quite straightforward:

$$n = \int_{all\ \mathbf{v}} f(\mathbf{v}) d^3\mathbf{v} = \eta_s + \eta_u + \eta_m = \eta_s + 2\eta_u = 2\eta_o - \eta_s \tag{12a}$$

For the velocity, we find

$$n\mathbf{V} = \int_{all\ \mathbf{v}} \mathbf{v} f(\mathbf{v}) d^3\mathbf{v} = \mathbf{j_s} + \mathbf{j}_u + \mathbf{j}_m = \mathbf{j_s} + 2\eta_u \mathbf{V}$$
$$= \mathbf{j_s} + (2\eta_o - 2\eta_s)\mathbf{V} = (\mathbf{j_s} - \eta_s \mathbf{V}) + (2\eta_o - \eta_s)\mathbf{V}$$
$$= (\mathbf{j_s} - \eta_s \mathbf{V}) + n\mathbf{V},$$

which can only be true if the first term on the right-hand side is zero, and this condition thus provides us with the means to estimate the bulk velocity **V**:

$$\mathbf{V} = \mathbf{j}_s / \eta_s \tag{12b}$$

Finally, the temperature can be determined:

$$\begin{aligned} \tfrac{1}{m} n\underline{\underline{\mathbf{T}}} &= \int_{all\ \mathbf{v}} (\mathbf{v}-\mathbf{V})(\mathbf{v}-\mathbf{V})\ f(\mathbf{v})\, d^3\mathbf{v} = \int_{all\ \mathbf{v}} \mathbf{vv}\ f(\mathbf{v})\, d^3\mathbf{v} - n\mathbf{VV} \\ &= \underline{\underline{\boldsymbol{\tau}}}_s + \underline{\underline{\boldsymbol{\tau}}}_u + \underline{\underline{\boldsymbol{\tau}}}_m - n\mathbf{VV} = \underline{\underline{\boldsymbol{\tau}}}_s + \underline{\underline{\boldsymbol{\tau}}}_u + \underline{\underline{\boldsymbol{\tau}}}_u + 4\eta_u \mathbf{VV} - 2\mathbf{V}\mathbf{j}_\mathbf{u} - 2\mathbf{j}_\mathbf{u}\mathbf{V} - n\mathbf{VV} \\ &= 2\underline{\underline{\boldsymbol{\tau}}}_o - \underline{\underline{\boldsymbol{\tau}}}_s + (2\eta_o + \eta_s)\mathbf{VV} - 2(\mathbf{V}\mathbf{j}_o + \mathbf{j}_o\mathbf{V}) \end{aligned} \tag{12c}$$

The procedure implemented in the code is iterative. We first calculate the integrals η_o, $\mathbf{j}_o$, and $\boldsymbol{\tau}_o$ (Equations 11a-c), using the entire observed distribution (and substituting finite-difference summation for the integration). From these integrals we obtain a first estimate of the velocity (c.f., Equation 12b):

$$\mathbf{V}^{(0)} = \mathbf{j}_o / \eta_o \tag{13}$$

With this estimated velocity, we separate the observed velocity space into the symmetric and unbalanced parts by examining for each measurement point $\mathbf{v}$ whether or not its mirrored point ($2\mathbf{V}^{(0)}$-$\mathbf{v}$) also lies within the observed velocity space. With this partition, we calculate the sums for just the symmetric part (Equations 8a, 9a, and 10a), use Equation 12b to find the corresponding velocity, re-determine the symmetric part of the observation space, recalculate the sums for the new symmetric part, and continue this iteration until the derived velocity converges. In practice, we require either that the magnitude of $\mathbf{V}$ not change by more than 1% from the previous value or that a maximum of 15 iterations are completed.

When the final iterated value of $\mathbf{V}$ has been determined, we use the sums for the final symmetric portion of the observation space for η_s, $\mathbf{j}_s$, and $\boldsymbol{\tau}_s$. Combined with the values η_o, $\mathbf{j}_o$, and $\boldsymbol{\tau}_o$ we obtained on the first pass through the data, we then use Equations 12 to determine the desired moments.

With the temperature matrix determined according to Equation 12c, we then diagonalize it, using the JACOBI subroutine from *Numerical Recipes* [Press et al., 2001], obtaining the three eigenvalues and their corresponding eigenvectors. We find the eigenvalue that is most different from the other two and identify this with Tpara, and its associated eigenvector we take to be the symmetry axis of the distribution. In a perfect world, this would be the magnetic field direction. In practice, it is probably dominated by instrument-response effects that are not completely removed in the analysis. For Tperp, we average the remaining two eigenvalues, recording also their ratio.

II. *Finite-Difference Approximation to Moment Integrals*

For the numerical implementation of the integrals discussed above, we follow the development given by Thomsen et al. [1999]:

Calculation of the moments (Equations 1) involves integrating the phase space density, weighted by various functions of the particle velocity, over velocity space:

$$\begin{aligned} M_n &= \int f(\mathbf{v}')\, g_n(\mathbf{v}')\, d^3\mathbf{v}' \\ &= \int dv' \int d\phi' \int d\theta'\, v'^2 \sin\theta'\, f(\mathbf{v}')\, g_n(\mathbf{v}'). \end{aligned} \tag{14}$$

This integration refers to the velocity-space properties in the ambient medium (v',θ',ϕ'), which are not necessarily the same as those measured at the satellite (v,θ,ϕ). In particular, surface charging of the spacecraft causes incident particles to gain or lose energy as they pass through the potential sheath around the spacecraft, and the first step in evaluating these integrals is to identify the transformation between the measured properties (v,θ,ϕ) and the ambient properties (v',θ',ϕ'). The measured energy of a given particle, E, is related to its energy at infinity (i.e., outside the spacecraft sheath), E', by

$$E = E' - q\Phi_{sc}$$

where q is the particle charge, and Φ_{sc} is the spacecraft potential. Neglecting sheath asymmetries and focusing (i.e., we assume that only the particle's energy and not its direction of motion is altered by the potential), we have the relationships

$$v' = \sqrt{2(E + q\Phi_{sc})/m} \tag{15a}$$

$$\theta' = \theta \tag{15b}$$

$$\varphi' = \varphi \tag{15c}$$

Typically at Saturn, the spacecraft potential is positive since the overall charging is dominated by photoelectron emission. A positive potential can in principle be measured by looking for the signature of trapped photoelectrons in ELS (note, however, that in conditions of dense, cold plasma, such as Titan's ionosphere, or in eclipse conditions, such as the SOI ring crossing, the potential can go slightly negative, and then ELS can only tell that the potential is no longer positive). Eventually, the ELS determination will be the preferred method for obtaining Φ_{sc} for the SNG moments calculation. Currently, however, it must be input manually, and a single value (normally zero) is used for an entire run.

The weighting functions g_n needed for the moments in Equations 14 are separable functions of the three velocity-space coordinates:

$$g_n(\mathbf{v}') = V_n(v')\, \Theta_n(\theta')\, \Phi_n(\phi'),$$

where the functions V_n, Θ_n, and Φ_n for the moments of interest are listed in Table 1.

Under the assumption that the distribution function is uniform over a particular velocity-space element ($\Delta\theta'$, $\Delta\phi'$, $\Delta v'$), the integral moments M_n can be approximated as weighted sums of the phase space density over contiguous finite velocity-space elements:

$$M_n \approx M_n = \Sigma_i \Sigma_j \Sigma_k (f'_{ijk}) [\int_i dv' \, v'^2 \, V_n(v')] \times [\int_j d\theta' \, \sin\theta' \, \Theta_n(\theta')] [\int_k d\phi' \, \Phi_n(\phi')]$$

$$= \Sigma_i \Sigma_j \Sigma_k (f'_{ijk}) \, V_{ni} \, Q_{nj} \, F_{nk}. \qquad (16)$$

In this equation, f'_{ijk} is the phase space density of the particles with velocity $\mathbf{v}'$ in the ambient medium. However, by Liouville's theorem, the phase space density is conserved along dynamical trajectories, so

$$f'_{ijk} = f(\mathbf{v}') = f(\mathbf{v}) = f_{ijk},$$

where $\mathbf{v}$ and $\mathbf{v}'$ are related by Equations 15, and f_{ijk} is the phase space density measured at the instrument, i.e.,

$$f_{sijk} = \frac{C_{sijk}}{\tau \varepsilon_{si} G_j E_i^2 \alpha_s}. \qquad (17)$$

In Equation 17, C_{sijk} is the counts for species s measured in detector j at energy level i and azimuth k. The parameters in the denominator are

τ = IMS accumulation interval = 0.0625 s
$\alpha_s = (2/m_s^2) = 1.835\text{e}24 \, (m_p/m_s)^2 \, (\text{cm}^4/\text{eV}^2\text{s}^4)$
E_i = energy of level i (eV)
G_j = geometric factor of detector j = 1.5008e-3 $\text{cm}^2\text{sr eV/eV}$
ε_{si} = detection efficiency for species s at energy E_i
= (foil transmission)(dome grid trans)(MCP grid trans)(start efficiency)
= (0.66)(0.65)(0.9)(0.69) for SNG
= 0.266 (18)

The geometric factor G_j and the detection efficiency ε_{si} are subject to revision pending ongoing discussions and analysis, but the values given in (18) are the ones implemented in Revision 0 of the code. The values of G_j and ε_{si} are listed as part of the output of the code.

In Equation 16, $\int_i$ represents the integration over the ith v'-cell, with limits v'_{i1} to v'_{i2}, and similarly for $\int_j$ and $\int_k$. By Equations 15b and 15c, $\theta'_{j1} = \theta_{j1}$, $\theta'_{j2} = \theta_{j2}$, $\phi'_{k1} = \phi_{k1}$, and $\phi'_{k2} = \phi_{k2}$. Thus, the moment sums of Equation 16 may be written as

$$M_n = \Sigma_i \Sigma_j \Sigma_k f_{ijk}(v_i,\theta_j,\phi_{ik})\, V_{ni}\, Q_{nj}\, F_{nik}. \quad (19)$$

The integrated elements V_{ni}, Q_{nj}, and F_{nik} are listed in Table 2. Note that V_{ni} must still be evaluated at the free-space limits v'_{i1} and v'_{i2}, which are related to the energy channel edges according to Equation 15a, but this is the only place that the correction for the spacecraft potential needs to be made.

Because of the way CAPS is actuated, $\Delta\phi$ in the expressions for F_{nik} in Table 2 is not constant from measurement to measurement. Moreover, since the actuator may sweep back and forth over the same look direction during the interval used for a particular calculation, the azimuth is not necessarily a monotonic function of time, so the ϕ_{ik} need to be reordered before the corresponding $\Delta\phi$ are computed. These complications will be addressed below in Section III.h.

The sums in Equation 19 extend over all 8 detectors (*j*) and all azimuthal sectors (each corresponding to a single energy sweep, *k*). The sum over the energy channels, *i*, could be restricted to certain ranges, depending on the target population, but in the current implementation, the entire energy range is included.

III. *Computational Steps*

The steps involved in computing the numerical moments according to the above scheme are summarized in Figure 1 and described as follows:

a) Specify run parameters.
In addition to the date and time range, the user can specify the number of A-cycles to be included in each computed value of the moments. Normally, this would be selected to cover a full actuation cycle in order to have the best chance of catching the true centroid of the distribution. The user must also specify how many (and which) species to analyze. The default value is 2 (H+ and O+). Moreover, the method by which the SNG counts are to be partitioned into these species must be specified. The partition subroutine returns values of the fraction of counts at a given energy (F_i) that should be assigned to a given species (i). The options currently available in the code are:

Method #	Description
1	F_i = 1.0, all energies, all species
2	F_i hard-wired to TBD values
3	F_i determined by Reisenfeld TOF-ST analysis
4	F_i determined by Reisenfeld TOF-LEF analysis
5	for O+, F_i = 1 above E=4*$E_{H,corot}$, 0 otherwise for H+, F_i = 1 below $E_{H,corot}$, 0 otherwise

Method 5 is based on the common presence in the energy-time spectrograms of two distinct ion populations, separated at roughly 4*$E_{H,corot}$, with dominantly O+ or water-

group ions at the higher energies and H+ at the lower energies. We have used this method for our initial runs, pending more correct information from the TOF integrations.

b) Determine the telemetry mode.
This is necessary because the telemetry mode determines the number of energy and angle channels that are included in each A-cycle of data. This information also allows us to populate the energy-level matrix.

c) Invert the cross-talk matrix.
Laboratory calibrations and IMS observations in the solar wind indicate that there is cross-talk between the different IMS anodes, i.e., some fraction of particles that are incident from the nominal look direction of a given anode will be counted instead at one of the other anodes. One current explanation of this cross-talk [M. Shappirio, personal communication, 1/25/2005] is that the charge cloud emerging from the back of the Start MCP stack may at times be deflected into the wrong anode. Another possibility involves scattering of a fraction of the incident ions. Either way, we can account for the effect as follows. We assume that the observed counts in the jth detector are given by

$$C_j = \left[1 - \sum_{i \neq j} \alpha_{ij}\right] C'_j + \sum_{i \neq j} \alpha_{ji} C'_i \tag{20}$$

where C'_j is the true counts incident into detector j, and α_{ij} is the fraction of counts incident on detector j that are scattered into detector i. In matrix notation

$$\mathbf{C} = \mathbf{A} \cdot \mathbf{C}' \tag{21}$$

where

$$A_{ij} = \begin{Bmatrix} \alpha_{ji} & i \neq j \\ 1 - \sum_{l \neq j} \alpha_{lj} & i = j \end{Bmatrix} \tag{22}$$

From the observed counts, C, we can find the true counts, C', by inverting the coupling matrix **A**:

$$\mathbf{C}' = \mathbf{A}^{-1} \cdot \mathbf{C} \tag{23}$$

We can estimate the coefficients A_{ij} from laboratory or solar wind observations: If the beam is known to be coming into only one detector (say k), we can normalize the observed counts in the other detectors by the counts in the target detector k, according to Equation (20)

$$R_{jk} \equiv \frac{C_j}{C_k} = \frac{\alpha_{jk}}{\left[1 - \sum_{i \neq k} \alpha_{ik}\right]}$$

In terms of the ratios R_{jk}, the coupling coefficients are

$$\alpha_{jk} = \frac{R_{jk}}{\left[1 + \sum_{l \neq k} R_{lk}\right]} \tag{24}$$

Table 3 shows the average channel ratios R_{jk} derived from laboratory calibrations done with the IMS-FM at Los Alamos, as well as the resulting coefficients α_{jk}. When the cross-talk removal is turned on, we compute the matrix elements A_{ij} from these coefficients according to Equation 24 and invert the matrix **A** to obtain the matrix $\mathbf{A}^{-1}$ needed to sharpen the distribution according to Equation 23.

Steps a-c are performed only once at the initiation of each run of the code. The computation of the moments for each set of A-cycles begins with step d:

d) Obtain the needed ancillary data.
This includes the spacecraft position, velocity, and attitude, as well as the orientation of Saturn's spin axis.

e) Read specified number of A-cycles (data and actuator angles).
The counts data are placed in the matrix *C(icyc,i,j,k)*, where *icyc* is the A-cycle number, *i* is the energy level, *j* is the detector number, and *k* is the sweep number.

To do the calculation described above, each measurement needs to have associated with it the appropriate look direction, which is given by the polar angle of the relevant detector and the azimuth angle at the time of the measurement. The azimuth angle is derived from the actuator angles provided in the data record. However, only a limited number of actuator values are provided, and to obtain the azimuth of any particular measurement, we need to interpolate between the reported actuator values. Thus, in this step the actuator angles in the data file are read in and interpolated to associate a specific actuator angle with each energy level in each sweep. This interpolation is straightforward when the SNG data are not collapsed in azimuth, but more difficult when collapse is required by the telemetry rate. Our approach is a two-step process: First we interpolate linearly between the reported actuator values (4 or 32, depending on the telemetry) to fill a full 8 az x 64 en matrix of act values. Then we collapse this full matrix by averaging in the same manner as the corresponding counts matrix.

Finally, the derived actuator angles are converted to look azimuth in the spacecraft coordinate system according to the relation

Look Azimuth = 270° - Actuator Angle

f) Remove background.
Energetic radiation belt particles can penetrate the CAPS instrument and directly stimulate the microchannel plates, producing a background count rate that can be very substantial. For SNG, removal of the background is relatively straightforward, since its

contribution to the count rate of the instrument should be independent of the voltage setting on the plates and roughly independent of the azimuth. For various reasons, there might be some variation of the background from anode to anode, so background removal is done separately for each anode according to the following procedure.

For each A-cycle and at each energy level, the counts in each detector are averaged over all the separate azimuths. To improve the statistics, an additional average is done over every three energy levels. If the minimum such 3-channel average in detector *j* for that A-cycle is $<C_j>_{min}$, the average background for detector *j* is estimated to be

$$B_j = <C_j>_{min} + \mathrm{sqrt}(<C_j>_{min}). \qquad (25)$$

The sqrt term in Equation 25 is added under the assumption that for a Poisson-distributed background, the minimum observed rate is probably below the average by something like one standard deviation. The estimated average background B_j is then subtracted from all of the measured count-rate bins for detector *j*.

g) Sharpen distribution by removing cross-talk.
As described above in Section III.c, the background-corrected counts are sharpened according to Equation 23.

h) Perform species partition.
The total counts observed in each bin are partitioned according to the energy-dependent partition method specified in the input data (Section III.a):

$$CP(s,icyc,i,j,k) = F(s,i) \cdot C(s,i,j,k)$$

As illustrated in Figure 1, it is this species-partitioned counts matrix that is passed to the subroutine that does the actual numerical integrations.

i) Rank-order azimuth angles and determine $\Delta\phi$.
As discussed above in Section II, the formalism we are using requires that the azimuths be reordered to be monotonically increasing before the azimuth elements $\Delta\phi$ in Table 2 are computed. To do this, we use the sorting routine sort3 from *Numerical Recipes* [Press et al., 2001], which returns the rank-ordered list of azimuth values and their corresponding A-cycle and azimuth index. We only need to do this for the first energy level of each sweep, since $\Delta\phi$ should be essentially the same for all the energy levels in a given sweep.

j) Smooth counts matrix in azimuth and fill distribution function matrix.
Because of the uneven sampling in azimuth caused by the actuator motion, it is possible that several points within the distribution being analyzed might lie quite close to each other in azimuth. This is certainly the situation during intervals when the actuator was not moving, in which case the reported values of azimuth vary only by the uncertainties inherent in the actuator monitor readings. The contribution to the moments sums (Eq. 16) from each measurement is weighted by the azimuth separation $\Delta\phi$ between that

measurement and the next nearest azimuth. Thus, closely clustered measurements would tend to have little influence in the calculation. To rectify this, we smooth the observed distribution by replacing each value with the average of all the points that lie within 4.15 degrees in azimuth of it. This value is one-half of the intrinsic azimuthal response of the IMS detector. This smoothed value of the counts is then converted to phase space density according to Equation 17.

k) Compute the integrated moment elements (Table 2).
With $\Delta\phi$ determined as described in Section III.i, and the velocity bin-edges (v'_{i1} and v'_{i2}) corrected for the spacecraft potential according to Equation 15a, the moments elements V(n,i), Q(n,j), and F(n,i,k) in Table 2 are computed.

l) Compute moments.
With the integrated moments elements determined, the moment sums indicated in Equation 19 can be performed, and the various desired moments (Equation 1) estimated. On the first pass through the spectrum, all of the measurements are included, and these initial moments values are saved for later use in the calculation and are also part of the output produced by the code. From there on, the iterative procedure described in Section I is followed, until the derived velocity is unchanged to within the specified tolerance (1%) or until a specified maximum number of iterations (15) have been done. In the latter case, the reported number of iterations is set to -15. Both the initial moments values and the final ones are then reported back to the main program.

m) Convert to Saturn coordinates.
The moments returned from the subroutine, as described above, were computed in the spacecraft frame. Upon return to the main program, the vector quantities (the velocities and the symmetry axes derived from diagonalizing the temperature matrix) are rotated into the J2000 coordinate system. To obtain the flow velocity in inertial coordinates, the spacecraft velocity is added to the rotated velocity. Finally, the flow components in an inertial, Saturn-centered, equatorial frame (v_r, v_ϕ, v_θ) are determined.

IV. *Caveats*

There are a number of areas of concern regarding the moments derived from SNG data according to the program described above.

a) None of the various species-partition methods is fully satisfactory. Even method 5, based on TOF analysis, can be significantly in error if time variations in the spectra and composition occur on a shorter time scale than the interval required to accumulate statistically significant counts in a TOF spectrum. Note, however, that the entire formalism described above is also applicable directly to the IMS-IONS data product, where the species identification has already been done onboard.

b) The derived velocity will by construction lie within the instrument field of view. When the FOV actually encompasses the flow velocity, this is not a problem. But when the flow is not directly into the instrument, the returned values will not be correct.

c) The method is predicated on the actuation of the instrument back and forth across the distribution. When CAPS is not actuating, the interative scheme will fail. The analysis will still return the initially-derived values of the moments, but the reported direction of the flow velocity will simply correspond to the look direction of the instrument. Furthermore, the density will be much underestimated because the initial moments are just the sum over the small slice of the distribution that is actually observed. To provide a rough way to correct for this underestimate, the code returns the nominal range of azimuth that is included in the calculation (the minimum and maximum azimuth values encountered). Combined with the reported temperatures in the v and θ directions and an assumption about the Maxwellian nature of the distribution, a density correction factor can be estimated. However, a more sophisticated approach than the numerical integration employed here is clearly called for under these circumstances.

d) Because of the $1/E^2$ dependence of the distribution function, the computed moments (at least for H+) are very strongly influenced by counts in the lowest energy channels, which are likely random background and difficult to remove completely. Therefore, the code zeroes out the channels below a specified energy value. This cutoff energy is one of the input parameters ("Number of energies to exclude") and for most of our runs is set at ~9 eV (channel # greater than 50, with channel 1 the highest energy). A lower value will need to be used in the innermost part of the magnetosphere, where the real signal descends to low energies.

V. *Reported Results*

The results of the above calculations are printed to an ASCII file, with a name of the form SNG_200430118_M0.txt. The header and contents of the output file are as follows:

Sample Header (lines demarcated by initial #)

```
# SNG MOMENTS
# October 27, 2004 DOY 301 0000 - 0600
#
# Generated: Thu Feb 10 08:36:12 MST 2005
#
# Input Parameters:
# Number of Acycles in each fit:       13
# Number of species to compute:        3
# Desired species:        3
# Partition Method:        5
# Start Date: (yyyydoy)      2004301
# Stop Date: (yyyydoy)      2004301
# Number of energies to exclude:       13.0000
#
# CODE: REV0.0
#
#
# Column headings
```

Parameters (1 line for each spectrum, parameters separated by 1 or more blank spaces, carriage return at end of line)

1. year
2. doy
3. Hour
4. Min
5. Sec
6. H_iterations Number of iterations in H+ calculation (-x if no convergence within x iter)
7. H_points_total Number of individual measurements in full initial H+ distribution
8. H_points_iter Number of individual measurements in final iterated H+ distribution
9. H_azimuth_min minimum azimuth included in H+ moments calculation (deg)
10. H_azimuth_max maximum azimuth included in H+ moments calculation (deg)
11. H_initial_density initial H+ density (cm-3)
12. H_initial_vx_sc x-component (s/c frame) of initial H+ flow velocity (km/s)
13. H_initial_vy_sc y-component (s/c frame) of initial H+ flow velocity (km/s)
14. H_initial_vz_sc z-component (s/c frame) of initial H+ flow velocity (km/s)
15. H_initial_Tmax max eigenvalue of diagonalized initial H+ temperature matrix (eV)
16. H_initial_Tmid middle eigenvalue of diagonalized initial H+ temperature matrix (eV)
17. H_initial_Tmin min eigenvalue of diagonalized initial H+ temperature matrix (eV)
18. H_iter_density iterated H+ density (cm-3)
19. H_iter_vx_sc x-component (s/c frame) of iterated H+ flow velocity (km/s)
20. H_iter_vy_sc y-component (s/c frame) of iterated H+ flow velocity (km/s)
21. H_iter_vz_sc z-component (s/c frame) of iterated H+ flow velocity (km/s)
22. H_iter_Tpara iterated H+ temperature eigenvalue parallel to inferred symm axis (eV)
23. H_iter_Tperp iterated H+ temp eigenvalue perpendicular to inferred symm axis (eV)
24. H_iter_Tperp_ratio ratio of T eigenvalues perpendicular to iterated H+ symmetry axis
25. H_iter_symax_xsc s/c x-component of iterated H+ symmetry axis
26. H_iter_symax_ysc s/c y-component of iterated H+ symmetry axis
27. H_iter_symax_zsc s/c z-component of iterated H+ symmetry axis
28. H_iter_velcheck (magnitude of H+ velocity change in last iteration)/(final H+ velocity)
29. O_iterations Number of iterations in O+ calculation (-x if no convergence within x iter)
30. O_points_total Number of individual measurements in full initial O+ distribution

31. O_points_iter Number of individual measurements in final iterated O+ distribution
32. O_azimuth_min minimum azimuth included in O+ moments calculation (deg)
33. O_azimuth_max maximum azimuth included in O+ moments calculation (deg)
34. O_initial_density initial O+ density (cm-3)
35. O_initial_vx_sc x-component (s/c frame) of initial O+ flow velocity (km/s)
36. O_initial_vy_sc y-component (s/c frame) of initial O+ flow velocity (km/s)
37. O_initial_vz_sc z-component (s/c frame) of initial O+ flow velocity (km/s)
38. O_initial_Tmax max eigenvalue of diagonalized initial O+ temperature matrix (eV)
39. O_initial_Tmid middle eigenvalue of diagonalized initial O+ temperature matrix (eV)
40. O_initial_Tmin min eigenvalue of diagonalized initial O+ temperature matrix (eV)
41. O_iter_density iterated O+ density (cm-3)
42. O_iter_vx_sc x-component (s/c frame) of iterated O+ flow velocity (km/s)
43. O_iter_vy_sc y-component (s/c frame) of iterated O+ flow velocity (km/s)
44. O_iter_vz_sc z-component (s/c frame) of iterated O+ flow velocity (km/s)
45. O_iter_Tpara iterated O+ temperature eigenvalue parallel to inferred symm axis (eV)
46. O_iter_Tperp iterated O+ temp eigenvalue perpendicular to inferred symm axis (eV)
47. O_iter_Tperp_ratio ratio of T eigenvalues perpendicular to iterated O+ symmetry axis
48. O_iter_symax_xsc s/c x-component of iterated O+ symmetry axis
49. O_iter_symax_ysc s/c y-component of iterated O+ symmetry axis
50. O_iter_symax_zsc s/c z-component of iterated O+ symmetry axis
51. O_iter_velcheck (magnitude of O+ velocity change in last iteration)/(final O+ velocity)
52. H_initial_vr radial component of initial H+ velocity in SSQ* frame (km/s)
53. H_initial_vphi azimuthal component of initial H+ velocity in SSQ* frame (km/s)
54. H_initial_vtheta polar component of initial H+ velocity in SSQ* frame (km/s)
55. H_iter_vr radial component of iterated H+ velocity in SSQ* frame (km/s)
56. H_iter_vphi azimuthal component of iterated H+ velocity in SSQ* frame (km/s)
57. H_iter_vtheta polar component of iterated H+ velocity in SSQ* frame (km/s)
58. H_iter_symax_x x-component of the iterated H+ symmetry axis (??? frame)
59. H_iter_symax_y y-component of the iterated H+ symmetry axis (??? frame)
60. H_iter_symax_z z-component of the iterated H+ symmetry axis (??? frame)
61. O_initial_vr radial component of initial O+ velocity in SSQ* frame (km/s)
62. O_initial_vphi azimuthal component of initial O+ velocity in SSQ* frame (km/s)
63. O_initial_vtheta polar component of initial O+ velocity in SSQ* frame (km/s)
64. O_iter_vr radial component of iterated O+ velocity in SSQ* frame (km/s)
65. O_iter_vphi azimuthal component of iterated O+ velocity in SSQ* frame (km/s)
66. O_iter_vtheta polar component of iterated O+ velocity in SSQ* frame (km/s)

67. O_iter_symax_x x-component of the iterated O+ symmetry axis (??? frame)
68. O_iter_symax_y y-component of the iterated O+ symmetry axis (??? frame)
69. O_iter_symax_z z-component of the iterated O+ symmetry axis (??? frame)
70. min(bkgd(*,0)) min value (over current A-cycles) of bkgd subtracted from anode 1
71. max(bkgd(*,0)) max value (over current A-cycles) of bkgd subtracted from anode 1
72. min(bkgd(*,1)) min value (over current A-cycles) of bkgd subtracted from anode 2
73. max(bkgd(*,1)) max value (over current A-cycles) of bkgd subtracted from anode 2
74. min(bkgd(*,2)) min value (over current A-cycles) of bkgd subtracted from anode 3
75. max(bkgd(*,2)) max value (over current A-cycles) of bkgd subtracted from anode 3
76. min(bkgd(*,3)) min value (over current A-cycles) of bkgd subtracted from anode 4
77. max(bkgd(*,3)) max value (over current A-cycles) of bkgd subtracted from anode 4
78. min(bkgd(*,4)) min value (over current A-cycles) of bkgd subtracted from anode 5
79. max(bkgd(*,4)) max value (over current A-cycles) of bkgd subtracted from anode 5
80. min(bkgd(*,5)) min value (over current A-cycles) of bkgd subtracted from anode 6
81. max(bkgd(*,5)) max value (over current A-cycles) of bkgd subtracted from anode 6
82. min(bkgd(*,6)) min value (over current A-cycles) of bkgd subtracted from anode 7
83. max(bkgd(*,6)) max value (over current A-cycles) of bkgd subtracted from anode 7
84. min(bkgd(*,7)) min value (over current A-cycles) of bkgd subtracted from anode 8
85. max(bkgd(*,7)) max value (over current A-cycles) of bkgd subtracted from anode 8

*SSQ frame = inertial Saturn-centered equatorial coordinate system

Acknowledgments
We thank the other members of the CAPS team for their assistance and patience during the development of this analysis. This work was supported by NASA through Order Number W-19,289 to Los Alamos National Laboratory.

References

Press, W. H., S. A. Teukolsky, W. T. Vetterling, and B. P. Flannery, *Numerical Recipes in Fortran 77, the Art of Scientific Computing,* second edition, Cambridge University Press, Cambridge, 2001.

Thomsen, M. F., E. Noveroske, J. E. Borovsky, and D. J. McComas, Calculation of Moments from Measurements by the Los Alamos Magnetospheric Plasma Analyzer, Los Alamos Report, LA-13566-MS, May, 1999.

Table 1. Moment Functions

n	M_n	$V_n(v)$	$\Theta_n(\theta)$	$\Phi_n(\phi)$
1	n	1	1	1
2	nv_x	v	$\sin\theta$	$\cos\phi$
3	nv_y	v	$\sin\theta$	$\sin\phi$
4	nv_z	v	$\cos\theta$	1
5	nv_xv_x	v^2	$\sin^2\theta$	$\cos^2\phi$
6	nv_xv_y	v^2	$\sin^2\theta$	$\cos\phi \sin\phi$
7	nv_xv_z	v^2	$\sin\theta \cos\theta$	$\cos\phi$
8	nv_yv_y	v^2	$\sin^2\theta$	$\sin^2\phi$
9	nv_yv_z	v^2	$\sin\theta \cos\theta$	$\sin\phi$
10	nv_zv_z	v^2	$\cos^2\theta$	1

Table 2. Integrated Moment Elements

n	M_n	V_{ni}	Q_{nj}	F_{nik}
1	n	$(v'_{i2}{}^3 - v'_{i1}{}^3)/3$	$\cos\theta_{j1} - \cos\theta_{j2}$	$\Delta\phi$
2	nv_x	$(v'_{i2}{}^4 - v'_{i1}{}^4)/4$	$\Delta\theta/2 - (\sin2\theta_{j2} - \sin2\theta_{j1})/4$	$2\cos\phi_{ik} \sin(\Delta\phi/2)$
3	nv_y	V_{2i}	Q_{2j}	$2\sin\phi_{ik} \sin(\Delta\phi/2)$
4	nv_z	V_{2i}	$(\sin^2\theta_{j2} - \sin^2\theta_{j1}) / 2$	F_{1ik}
5	nv_xv_x	$(v'_{i2}{}^5 - v'_{i1}{}^5)/5$	$[\cos\theta_{j1} (\sin^2\theta_{j1} + 2)$ $- \cos\theta_{j2} (\sin^2\theta_{j2} + 2)] / 3$	$\Delta\phi/2 + (1 - 2\sin^2\phi_{ik})$ $\cdot \sin(\Delta\phi/2) \cos(\Delta\phi/2)$
6	nv_xv_y	V_{5i}	Q_{5j}	$2 \sin\phi_{ik} \cos\phi_{ik}$ $\cdot \sin(\Delta\phi/2) \cos(\Delta\phi/2)$
7	nv_xv_z	V_{5i}	$(\sin^3\theta_{j2} - \sin^3\theta_{j1}) / 3$	F_{2ik}
8	nv_yv_y	V_{5i}	Q_{5j}	$\Delta\phi/2 - (1 - 2\sin^2\phi_{ik})$ $\cdot \sin(\Delta\phi/2) \cos(\Delta\phi/2)$
9	nv_yv_z	V_{5i}	Q_{7j}	F_{3ik}
10	nv_zv_z	V_{5i}	$(\cos^3\theta_{j1} - \cos^3\theta_{j2}) / 3$	F_{1ik}

Table 3. Cross-Talk Coefficients from Laboratory Calibrations

|j-k|	R_{jk}	α_{jk}
0	1.0	0.748
1	0.135	0.101
2	0.0199	0.015
3	0.00915	0.007
4	0.00469	0.004

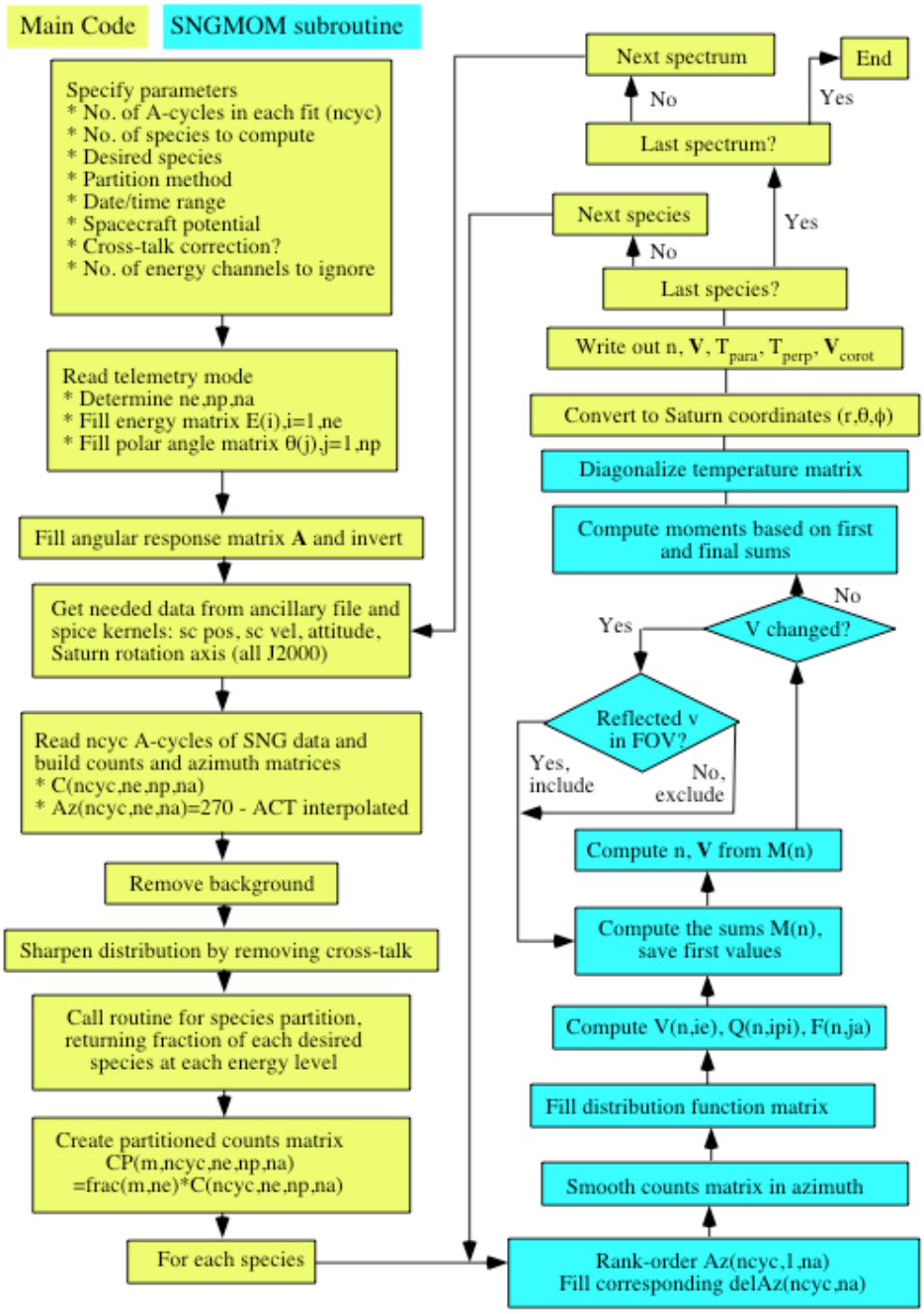

Figure 1. Flow chart for numerical moments computation from CAPS/IMS-SNG.